International Journal of Thermofluid Science and Technology (2023)
Volume 10, Issue 2, Paper No. 100202
https://doi.org/10.36963/IJTST.2023100202
Research Article

Unsteady flow and heat transfer characteristics over the rounded and square leading-edge plate

Channarong Wantha*

Energy Technology and Heat Transfer Enhancement Lab., Department of Agricultural Engineering, Faculty of Engineering, Rajamangala University of Technology Thanyaburi, Thanyaburi, Pathum Thani 12110, Thailand.

ATICLE INFO

Received: 25 Feb. 2023;
Received in revised form:
20 May 2023;
Accepted: 27 May 2023;
Published online:
28 May 2023

Keywords:
CFD
Heat transfer
Numerical analysis
Separated flow
Unsteady flow

ABSTRACT

The influences of the shape of the leading edge of the upstream plate on the transition region from steady laminar flow to unsteady flow, as well as the heat transfer from these leading edges, were numerically studied. The calculations were performed using the finite volume method in two-dimensional domains in a low Reynolds number regime with a constant incoming flow. The results show that von Kármán vortex shedding patterns start behind the rounded upstream plate at a low Reynolds number of 114. When the leading edge of the upstream plate is square, the plate experiences flow separation and the flow become unsteady at higher Reynolds numbers of around 400. The mean Nusselt number of the upstream plate increases by approximately 179% and 213% for square and rounded leading edges, respectively, for Reynolds numbers ranging from 100 to 700.

1. Introduction

Compact heat exchangers are used in various applications, including radiator and air conditioners, as well as for cooling electronic devices. This type of heat exchanger is designed with flat plate segments arranged in the flow direction to enhance thermal performance at low Reynolds numbers [1]. The rate of heat transfer of a compact heat exchanger can also be improved using surface interruption, which resets the boundary layer growth at each corner of the leading edge of plate [2, 3]. A number of studies have been conducted to explore various methods for improving the characteristics of separated and reattached flow over a blunt flat plate [4-8]. Ota et al. [9-11] pioneered this field by studying the flow characteristics of separation, reattachment, and rate of heat transfer under high Reynolds numbers on a blunt flat plate while also examining the effects of the nose shape of the plate on flow and heat transfer rates. It is important to note that the separation, recirculation, and reattachment feature of the flow is frequently an unfavorable result of the surface interruption, causing the friction factor to increase more than the Nusselt number [12]. The sharp corner of the plate caused separation flow at the leading edge [13], resulting in separation bubbles with no heat transfer benefit [14, 15]. Flow separation and heat transfer behavior are two fluid flow problems that have attracted research attention because they occur frequently in various engineering applications, including electronics heat sinks,

*Corresponding e-mail: cwantha@rmutt.ac.th (C.Wantha).

Nomenclature

b	plate thickness, m	S/L	dimensionless spacing between plates
Br	blockage ratio, Br = b/H	T	temperature, K
f	frequency of vortex shedding, Hz	U	inlet flow velocity, m/s
h	heat transfer coefficient, W/m^2 K	x	coordinate, distance from the leading edge
H	height of the domain, m		of the plate, m
j	Colburn factor	y	coordinate, m
k	thermal conductivity, W/m K	*Greek symbols*	
L	plat length, m	ρ	density, kg/m^3
L/b	dimensionless plate length	α	thermal diffusivity, m^2/s
L/r	dimensionless plate radius	ν	kinematic viscosity, m^2/s
Nu	Nusselt number	*Subscripts*	
Pr	Prandtl number	o	inlet
r	radius, m	b	plate thickness
Re	Reynolds number, Re = Ub/ν	i	velocity components
St	Strouhal number	x	local value
S	plate spacing	mean	mean value

chips on a board, blades, wings, sails, and buildings [16, 17]. Notably, these applications each have a different shape, which complicates their analysis. Yanaoka et al. [18] used two-dimensional (2D) and three-dimensional (3D) numerical simulations to investigate the flow and heat transfer characteristics over a blunt flat plate placed inside a square channel in a laminar uniform flow. Their 2D and 3D analyses showed that the transition from steady to unsteady flow occurs at different Reynolds numbers, with the 3D analysis occurring at a lower Reynolds number. Chatterjee et al. [19] conducted a numerical investigation of the effect of the shape of the curved and flat surfaces of a semicircular cylinder on the unsteady flow and heat transfer characteristics observed in laminar flow. They concluded that the shape surface facing the flow affects both the heat transfer rate and the frequency of vortex shedding. Chatterjee and Mondal [20] subsequently studied the unsteady mixed convective heat transfer characteristics of two square cylinders arranged in tandem in a laminar flow condition and revealed that the Nusselt number increased with the Reynolds number and the Richardson number, while the Richardson number also influenced the drag and lift coefficients. Chatterjee and Chaitanya [21] analyzed flow and heat transfer in tandem circular cylinders rotating at Re=100, comparing the impact of different spacings using two-dimensional numerical simulations. They discovered that cylinder spacing impacts the critical rotation rate. Regardless of gap spacing, isothermal and vortices behave in unstable ways when there is no rotation. Increasing the cylinder's rotational speed also results in a reduction in heat transfer. Chaitanya and Chatterjee [22] conducted further research on tandem circular cylinders by rotating the upstream and downstream cylinders in opposite directions at Re=100. They found that counterrotation stabilizes the flow field around the cylinders, which changes the characteristics of fluid flow and heat transfer. Chaitanya et al. [23] investigated the effect of cross-thermal buoyancy on flow transitions around side-by-side cylinders at Reynolds numbers ranging from 10 to 40. They found that heat transfer from both cylinders increases as the Reynolds number increases. Dey and Das [24] studied the flow around a triangular solid (thorn) fixed to a square cylinder and observed that the thorn length and inclination angle affected the drag and lift coefficients. A numerical study by Rastan et al. [25] on vortex shedding from a bluff body with cross-sections ranging from square to normal flat plates revealed significant effects on the critical Reynolds number of vortex shedding due to the cross-sectional aspect ratio of the bluff body. As a result, the separation of the flow above the plate must be taken into consideration when

designing the surface of the plate. Laminar boundary layer separation caused by the square leading edge of a plate is common in many forms of compact heat exchangers; however, when the leading edge of an upstream plate is rounded, the extent to which the flow and heat transfer mechanisms are similar, including throughout the transition process from steady to unsteady flow, remains unclear. The aim of this study was to numerically study the flow behavior and heat transfer characteristics of two flat plates, one in which the upstream plate lacked sharp edges and the other in which the upstream plate had a square leading edge. The conditions for the onset of the transition from steady to unsteady laminar flow regime between a pair of flat plates were investigated. Additionally, the behavior of the flowing and the Nusselt number was studied under the laminar flow regime. In this numerical analysis, the distance between the plates is fixed as S/L = 2.36. Air is used as working fluid with a Prandtl number of 6.14, and a uniform flow with a Reynolds number ranging from 100 to 700 is used. The results of this study should contribute to a better of flow behavior and heat transfer rates through interrupted plates and offer increased clarity regarding significant edge effects.

Table 1 Geometric and flow parameters.

Plate geometry	***S/L***	***L/b***	***L/r***	**Re$_b$**
Rounded edge	2.36	3.96	10.6	100-700
Square edge	2.36	3.96	-	100-700

2. Computational method

2.1 Computational domain

The physical problem considers two plates of equal length and thickness (length L, and thickness b) in a uniform flow of velocity U_o and temperature T_o. The two plates are arranged in configuration on the central axis of a computational domain as shown in Fig. 1. The blockage ratio of 2D computational domain of the problem was defined by Br (%) = b/H, where H is the distance between the upper and lower boundaries and b is the plate thickness. A blockage ratio (Br) of 4.2% was used in the computations. The domain consisted of an upstream plate located 3b away from the inlet boundary; the total domain length, at which the flow was fully developed, was 42b. The spacing between the two plates was a constant value of S/L=2.36. The flat plates were designed with a thickness, b, of 3.2 mm and a length, L, of 12.7 mm. The upstream plates had the same length and thickness but two different shapes; one had a rounded leading edge with a radius of 1.2 mm, and the other had a square leading edge. Table 1 shows the geometrical details of two different leading edges used in the study, whose plate dimensions are in accordance with the experimental study conducted by Roadman et al. [26].

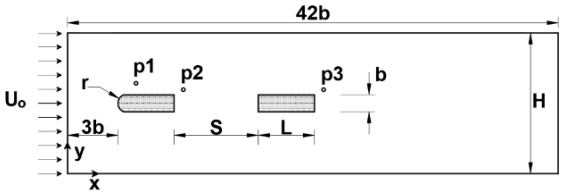

Fig. 1. Flow configuration and computational domain.

2.2 Governing equations

The flow in this study was assumed to be a 2D, incompressible, and unsteady laminar flow. The viscosity, density, and thermal properties of the fluid remained constant.

Furthermore, viscous dissipation was neglected. As a result of these assumptions, numerical simulations were carried out by solving time-dependent, continuity, momentum, and energy equations. The governing equations were as follows [27-29]:

$$\frac{\partial u_i}{\partial x_i} = 0 \tag{1}$$

$$\frac{\partial u_i}{\partial t} + \frac{\partial u_i u_j}{\partial x_j} = -\frac{1}{\rho}\frac{\partial \rho}{\partial x_i} + \nu \frac{\partial^2 u_i}{\partial x_j^2} \tag{2}$$

$$\frac{\partial T}{\partial t}+\frac{\partial u_j T}{\partial x_j}=\alpha\frac{\partial^2 T}{\partial x_j^2} \quad (3)$$

Where $i, j=1-3$; x_1, x_2 and x_3 represent the streamwise, cross-stream, and spanwise directions, respectively. u_1, u_2 and u_3 represent the corresponding resolved velocity components [30]. While ρ, ν, and α are density, kinematic viscosity, and thermal diffusivity, respectively.

2.3 Boundary conditions

The governing equations of (1)–(3) were solved in the computational domain shown in Fig. 1 using Fluent CFD software. Boundary conditions play an important role in the analysis and were categorized as follows:

Inlet: uniform flow ($u=U_o$, $v=0$ and $T=T_o$)

Outlet: Assuming the flow parameter did not vary in the x-direction.

Plate: Constant heat flux for energy; no-slip velocity conditions were imposed.

Upper and lower ends: Periodic boundary conditions is given by [31]

$$u(x,H)=u(x,0) \quad (4)$$

$$v(x,H)=v(x,0) \quad (5)$$

$$T(x,H)=T(x,0) \quad (6)$$

The air was used as working fluid with the Prandtl number $(\mathrm{Pr}=\nu/\alpha)$ remained constant at 6.14.

2.4 Numerical methods and description of the simulations

The simulations were carried out on a staggered grid using the commercial CFD software Fluent, which utilizes the finite volume method. The second upwind differencing scheme (USD-2) was used to discretize the convective and diffusive terms. The SIMPLE algorithm was used to find the solution, and the second-order implicit solution method was used to confirm calculation accuracy. The numerical simulations were carried out at Reynolds numbers ranging from 100 to 700 corresponding with the laminar flow. A convergence criterion was set to less than 10^{-6}. Table 1 shows the examined simulation cases.

2.5 Data acquisition

The Reynolds number, based on plate thickness, was calculated by:

$$\mathrm{Re}_b=\frac{U_o b}{\nu} \quad (7)$$

where b is the thickness of the plate.

The time-averaged local Nusselt number was expressed as:

$$\bar{N}u_x=\frac{\bar{h}_x b}{k} \quad (8)$$

where $\bar{h}_x$ is the time-averaged local heat transfer coefficient.

The mean Nusselt number was expressed as:

$$Nu_{mean}=\frac{1}{\Delta x}\int_{x_1}^{x_2}\bar{N}u_x dx \quad (9)$$

2.6 Mesh design and independence tests

This study employed non-uniform mesh distributions in the *x* and *y* directions, as shown in Fig. 2. The meshes were refined around the leading edge of each plate; i.e., they were refined around areas with high gradients. Conversely, a less refined mesh was used in areas with low gradients. A triangular mesh was formed around the upstream edge of the rounded plate, as shown in Fig. 3, while a rectangular mesh was used for the upstream plate with the square leading edge, as shown in Fig. 2. In this study, four different grids were used to study the effect of grid density on the calculation results for the mean Nusselt number of an upstream plate, as shown in Table 2. A grid independence test was performed for a Reynolds number of 793 (based on the plate length). The results show that the mean Nusselt number of the square and round leading edges was sensitive to the grid size. However, the deviations of the mean Nusselt number between the grids of case 3 and case 4 for both the square leading edge and the round leading edge were only 0.492% and 0.315%, respectively.

Table 2 Grid independence tests.

Geometry	Grid case	Grid number	Mean Nusselt number (Nu_L)	Relative error (%)
Rounded edge	Case 1	7,432	46.056	5.331
	Case 2	18,651	44.740	2.322
	Case 3	29,842	43.863	0.315
	Case 4	74,605	43.725	baseline
Square edge	Case 1	7,741	40.938	5.516
	Case 2	19,428	39.496	1.798
	Case 3	31,086	38.989	0.492
	Case 4	77,715	38.798	baseline

Thus, a total of 31,086 and 29,842 nodes were used for square and rounded leading edges, respectively, in the computational domain to simulate the study of flow and heat transfer. In addition, independent grid validation results showed that using these non-uniform grid structures for calculations was reliable and reduced computation time for consumers.

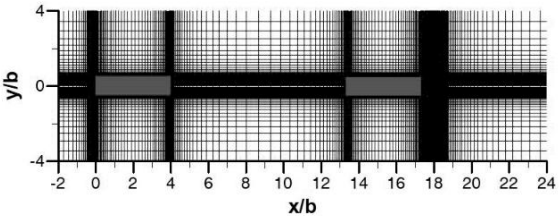

Fig. 2. Non-uniform computational mesh around two plates.

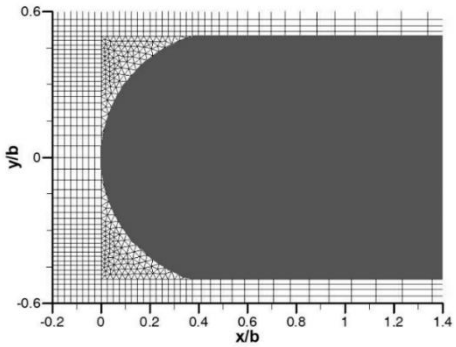

Fig. 3. Enlarged view of the mesh around the rounded leading edge.

2.7 Validation

The numerical method described above was validated using the well-known theoretical correlation for laminar flow over a flat plate as shown in Eq. (10). This correlation was used to calculate the mean Nusselt number for fluid flow along a horizontal flat plate at a constant surface temperature, given by [32].

$$Nu_{mean} = 0.664\,\mathrm{Re}_L^{1/2}\,\mathrm{Pr}^{1/3} \qquad (10)$$

Equation (10) is applicable for $\mathrm{Re}_L < 5\times10^5$, $\mathrm{Pr} > 0.6$.

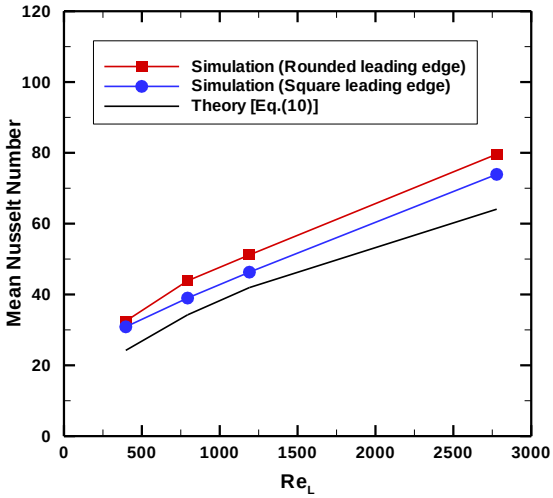

Fig. 4. Comparison between theory and numerical simulations of single plate

The average Nusselt number, based on the plate length, was calculated using a non-uniform grid distribution of case 3 (Table 2) that had been independence-grid checked. Fig. 4 shows a comparison of the mean Nusselt numbers in the upstream plates versus the Reynolds counts for both the numerical results from the present study and the theoretical correlation results for square-edged and rounded leading edges.

The results showed that the numerical simulation results clearly followed the same trend as the theoretical results, with good agreement between the theoretical and simulation results of a flat plate with a square leading-edge nose. For the simulation results of a square leading edge, the maximum deviation was about 6.857%. Nevertheless, for the simulation results of a rounded leading edge, the maximum deviation was about 8.533%. This deviation difference can be explained by the numerical diffusion of the solver or vortex, as well as the flow separation at the leading edge.

3. Results and discussion

3.1 Effect of Reynolds number on flow over the two plates in a channel

At a low Reynolds number of about 100, flow separation and vortex shedding around plates did not occur on either the rounded or square-edged simulations, as illustrated in Fig. 5. The flow characteristic remained almost steady; the influence of the viscous forces was greater than that of the inertial forces.

Figure 6 shows a Reynolds number of 114 over the plates with a rounded leading edge; the flow's behavior became unsteady. More specifically, the vortices were formed behind the downstream plate; they then periodically separated from either side, forming a von Kármán vortex street. Thus, the critical of transition from a steady to an unsteady flow is approximately Reynolds number 114 for a flow over an upstream plate with rounded edges under inline flow for S/L=2.36 and L/b=3.96. These results are in agreement with the flow visualization results obtained by Roadman et al. [26]. With further increases of the Reynolds number from the critical of 114 to around 200, the flow over the rounded upstream plate became unsteady, vortices elongated, and some even shed in the direction of the flow, as shown in Fig. 7. Conversely, at a Reynolds number of 200 on a square leading edge, no vortices were generated, as shown in Fig. 8. However, the results of calculations using a Reynolds number of 400 showed that the flow eventually became unsteady and that vortex shedding around the plate appeared.

The results of calculations for the rounded and square edged plates at the same Reynolds number showed that the rounded edge obstructed flow and flow separation, reattachment length founded on an upstream plate's top and bottom surfaces, while the square edged plate allowed for the easy occurrence of flow separation and reattachment; this is because the square-edged plated has sharp corners and the flow cannot turn, as shown in Fig. 9.

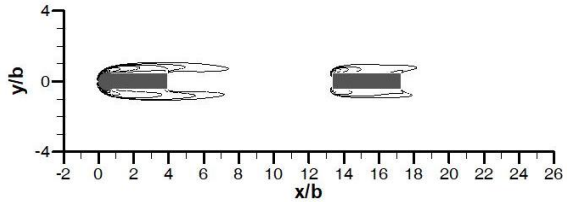

Fig. 5. Instantaneous vorticity contours for a flow past the rounded leading-edge plate at Re_b=100.

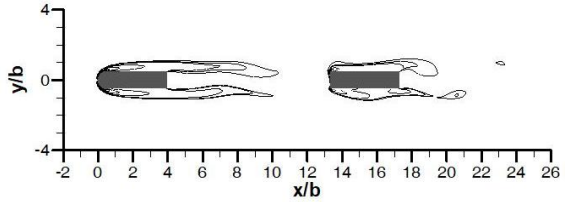

Fig. 6. Instantaneous vorticity contours for a flow past the rounded leading-edge plate at Re_b=114.

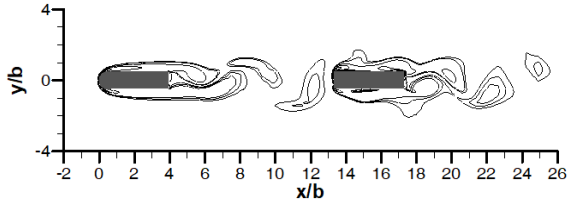

Fig. 7. Instantaneous vorticity behind the rounded leading-edge plate in a channel at Re_b= 200.

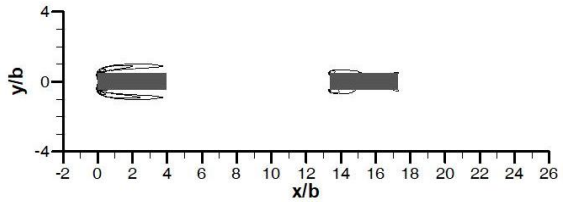

Fig. 8. Instantaneous vorticity contours for a flow past the square leading-edge plate at Re_b=200.

For the flow behavior of interrupted flat plates when the upstream plate is rounded, the

calculation showed that the vortices migrate to the back of the plate. The flow separation between top and bottom surface of plate reformed at the back of each plate, resulting in Kelvin-Helmholtz flow type instability, as shown in Fig. 7, which is similar to flowing through an airfoil.

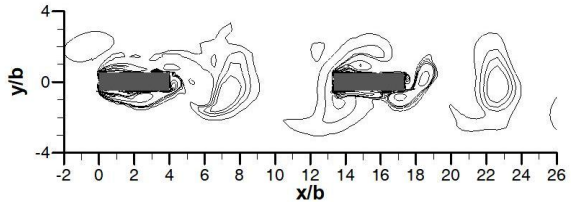

Fig. 9. Instantaneous vorticity behind the square leading-edge plate in a channel at Re_b= 700.

3.2 Frequency analysis

Figures 10 to 12 show the power spectrum density obtained using Fast Fourier Transform analysis (FFT) on velocity data according to the recorded position of p1 (for x=0.945b, y=1.0b), p2 (for x=2.34b, y=0.5b), and p3 (for x=2.34b, y=0.5b); these positions are shown in Fig.1. The dimensionless frequency, defined as the Strouhal number of vortex shedding, was expressed as:

$$St = \frac{bf}{U_o} \tag{11}$$

where f is the frequency of vortex shedding in the plates.

The highest peaks in each power spectrum graph correspond to the vortex shedding frequency. First, at p1's location, which is near the top surface of the upstream plate, under Reynolds number of 700, the results show that the Strouhal number peaked at approximately 0.0021 for a square-edged plate and 0.0032 for a rounded edge plate, as shown in Fig. 10. This result clearly shows that a square upstream plate leads to a more unstable flow than the rounded plate, which created a small flow separation.

Figure 11 illustrates the power spectrum density at p2; it can be seen that a square-edged upstream plate has a power spectrum density peak at a Strouhal number of around 0.0021 which is the same as p1; however, the power spectrum density is lower. When the upstream plate is rounded, the power spectrum density is highest at a Strouhal number of 0.0032; power spectrum density was also greater than at p1.

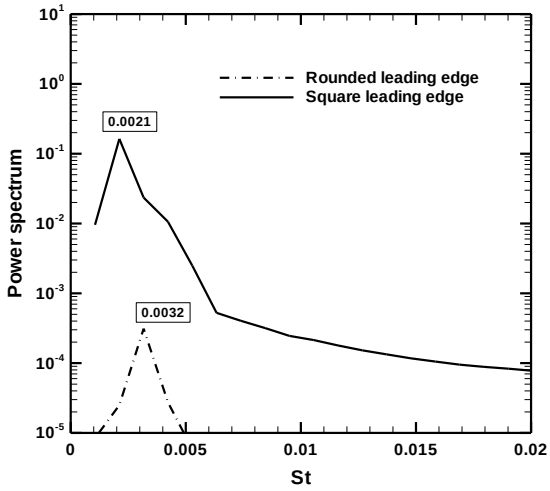

Fig. 10. The Strouhal number of the location of p1 at Re_b=700.

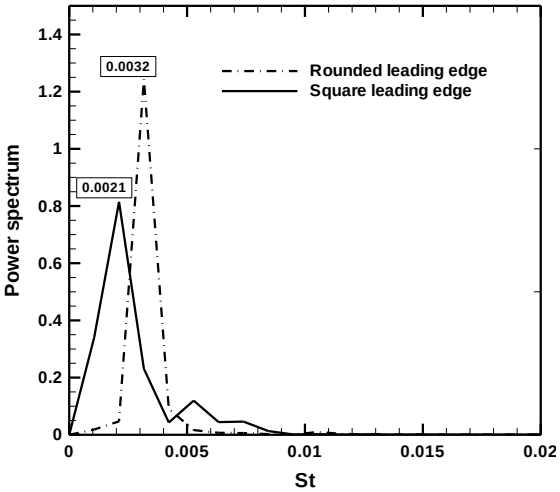

Fig. 11. The Strouhal number of the location of p2 at Re_b=700.

Figure 12 shows the power spectrum density and Strouhal number at p3 behind of a downstream plate. The power spectrum density is highest at the Strouhal number of 0.0011 and 0.0021 for the square and rounded edges, respectively. The calculations show that flowing over a rounded-edged plate creates a stronger von Kármán vortex street behind the plate than flowing over a square leading edge.

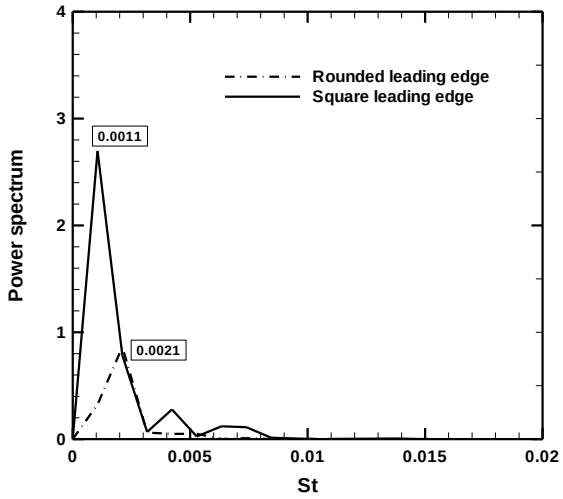

Fig. 12. The Strouhal number of the location of p3 at Re_b=700.

3.3 Heat transfer

In this study, the specified heat flux along the plate surface remained constant so that as the temperature of the plate wall decreased, both the heat transfer rate and the local heat transfer coefficient increased. Fig. 13 shows the distribution of the local time-averaged Nusselt number along the surface of the upper plate for different Reynolds numbers. As shown in this graph, the Nusselt number sharply increased at each Reynolds number due to the strong shear layer near the leading edge of the plate. The peak Nusselt number neighborhood of the leading edge is due to the flow separations occurring there; however, the local Nusselt number decreased continuously as distance increased, and then slightly increased again at the end edge of each plate due to the instability mechanisms of the free shear layers downstream of the plate.

The total averaged Nusselt number, which is expressed in terms of the dimensionless Colburn j factor, is a calculation of the average heat transfer over the upper and lower surfaces of the upstream plate, as shown in Fig. 14.

The Colburn j factor is defined as:

$$j = St\,\mathrm{Pr}^{2/3} = \frac{Nu}{\mathrm{Re}\,\mathrm{Pr}^{1/3}} \tag{12}$$

The calculated results are compared to the correlation by Kays, which is expressed in Eq. (13) (see Manglik et al.[33]) for laminar flow over interrupted plates:

$$j = 0.665\,\mathrm{Re}_b^{-0.5} \tag{13}$$

The results indicated that increases in the Reynolds number caused a decrease in the j factor, which is in line with the results of Eq. (13) and is caused by a decrease in the Stanton numbers (St=Nu/RePr). According to the calculations, increasing the Reynolds number from 100 to 700 increases the mean Nusselt number of the upstream plate by approximately 179% and 213% for square and rounded leading edges, respectively.

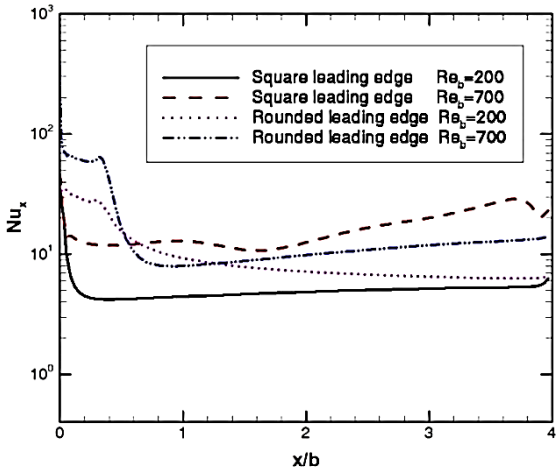

Fig. 13. Effect of leading edges on Nusselt number distributions on the upstream plate.

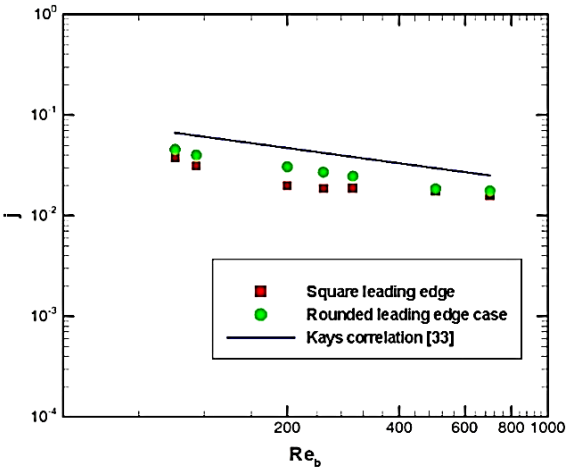

Fig. 14. Variations of the Colburn j-factor with the Reynolds number.

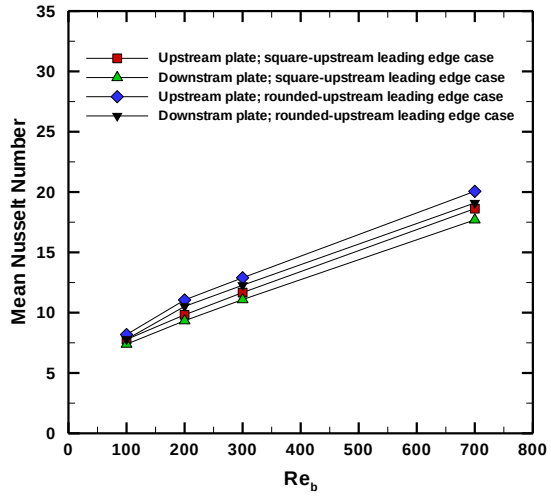

Fig. 15. The Nusselt number of upstream and downstream plates with the Reynolds number.

Fig. 15 illustrates the mean Nusselt number of the upstream and downstream plates in the flow direction. The results showed that the shape of the upstream plate had little effect on the downstream plate, possibly due to the spacing of the two plates used for simulation.

4. Conclusions

The flow behavior and heat transfer for two different plates with constant spacing along the flow direction were numerically investigated. This study focused on the effects of the upstream plate's leading edges, whether square or rounded, on the transition region from steady laminar flow to unsteady flow, as well as heat transfer from these leading edges. Two-dimensional simulations were performed using a low Reynolds number regime with a constant incoming flow. The calculations revealed a difference in the transition from steady to unsteady flow between the square and round leading edges. When the upstream plate was rounded, the transition from steady to unsteady flow occurred at a low Reynolds number of around 114, and von Kármán vortex shedding occurred near the back of the plate. However, no periodic vortex shedding was observed at those Reynolds numbers in the case of the square leading edge. As the Reynolds number approached 400, flow separation occurred at the leading edge of the square upstream plate, leading to unsteady flow. The results of the Strouhal number calculations showed that the upstream plate's square and rounded leading edges differed and that the flow was more unstable along the square leading edge than along the rounded leading edge. As the Reynolds number increased from 100 to 700, the mean Nusselt number of the upstream plate increased by approximately 179% and 213% for the square and rounded leading edges, respectively. However, further study is needed on lift coefficient signals during vortex shedding for a clearer understanding of interrupted flat plate flow transitions.

Acknowledgments

The author would like to thank Agricultural engineering department, Rajamangala University of Technology Thanyaburi, Thailand for their equipment support for this study.

References

1. Marty P, Michel F, Tochon P (2008) Experimental and numerical study of the heat transfer along a blunt flat plate. International Journal of Heat and Mass Transfer51:13-23DOI https://doi.org/10.1016/j.ijheatmasstransfer.2007.04.036
2. Mullisen RS, Loehrke RI (1986) A study of the flow mechanisms responsible for heat transfer enhancement in interrupted-plate heat exchangers. Journal of Heat Transfer108:377-385DOI https://doi.org/10.1115/1.3246933
3. Chakma JM, Abedin MZ (2021) Review on heat transfer enhancement by rectangular Fin. International Journal of Engineering Materials and Manufacture 6 DOI https://doi.org/10.26776/ijemm.06.02.2021.01
4. Lane JC, Loehrke RI (1980) Leading edge separation from a blunt plate at low Reynolds number. Journal of Fluids Engineering102:494-496DOI https://doi.org/10.1115/1.3240731
5. Zelenka RL, Loehrke RI (1983) Heat transfer from interrupted plates. Journal of Heat Transfer 105: 172-177 DOI https://doi.org/10.1115/1.3245537
6. Nakamura Y, Ohya Y, Ozono S, Nakayama R (1996) Experimental and

numerical analysis of vortex shedding from elongated rectangular cylinders at low Reynolds numbers 200-103. Journal of Wind Engineering and Industrial Aerodynamics65:301-308DOI https://doi.org/10.1016/S0167-6105(97)00048-2

7. Chai L, Xia GD, Wang HS (2016) Laminar flow and heat transfer characteristics of interrupted microchannel heat sink with ribs in the transverse microchambers. International Journal of ThermalSciences110:1-11DOI https://doi.org/10.1016/j.ijthermalsci.2016.06.029
8. Yifan D, Chuangxin H, Peng W, Yingzheng L (2020) Unsteady behaviors of separated flow over a finite blunt plate at different inclination angles. Physics of Fluids32:035111-035111DOI https://doi.org/10.1063/1.5143508
9. Ota T, Kon N (1974) Heat transfer in the separated and reattached flow on a blunt flat plate. Journal of Heat Transfer 96: 459-462DOI https://doi.org/10.1115/1.3450227
10. Ota T, Kon N (1979) Heat transfer in the separated and reattached flow over blunt flat plates —Effects of nose shape. International Journal of Heat and Mass Transfer22:197-206DOI https://doi.org/10.1016/0017-9310(79)90143-1
11. Ota T, Asano Y, Okawa J-i (1981) Reattachment length and transition of the separated flow over blunt flat plates. Bulletin of JSME 24: 941-947 DOI https://doi.org/10.1299/jsme1958.24.941
12. Shah RK, Sekuli DP (2003) Fundamentals of heat exchanger design John Wiley & Sons, Inc., Hoboken, NJ, USA
13. Fujiwara K, Sriram R, Kontis K (2020) Experimental investigations on the sharp leading-edge separation over a flat plate at zero incidence using particle image velocimetry. Experiments in Fluids 61: 205-205DOI https://doi.org/10.1007/s00348-020-03039-w
14. Djilali N (1994) Forced laminar convection in an array of stacked plates. Numerical Heat Transfer, Part A: Applications25:393-408DOI https://doi.org/10.1080/10407789408955956
15. Suksangpanomrung A, Djilali N, Moinat P (2000) Large-eddy simulation of separated flow over a bluff rectangular plate. International Journal of Heat and Fluid Flow21:655-663DOI https://doi.org/10.1016/S0142-727X(00)00057-6
16. Yaghoubi M, Mahmoodi S (2004) Experimental study of turbulent separated and reattached flow over a finite blunt plate. Experimental Thermal and Fluid Science29:105-112DOI https://doi.org/10.1016/j.expthermflusci.2004.02.003
17. Smith JA, Pisetta G, Viola IM (2021) The scales of the leading-edge separation bubble. Physics of Fluids 33: 045101 DOI https://doi.org/10.1063/5.0045204
18. Yanaoka H, Yoshikawa H, Ota T (2001) Numerical simulation of laminar flow and heat transfer over a blunt flat plate in square channel. Journal of Heat Transfer 124:8-16DOI https://doi.org/10.1115/1.1420715
19. Chatterjee D, Mondal B, Halder P (2013) Unsteady forced convection heat transfer over a semicircular cylinder at low Reynolds numbers. Numerical Heat Transfer, Part A: Applications 63: 411-429 DOI https://doi.org/10.1080/10407782.2013.742733
20. Chatterjee D, Mondal B (2013) Unsteady mixed convection heat transfer from tandem square cylinders in cross flow at low Reynolds numbers. Heat and Mass Transfer49:907-920DOI https://doi.org/10.1007/s00231-013-1133-z
21. Chatterjee D, Chaitanya NVVK (2020) Convective transport around two rotating tandem circular cylinders at low Reynolds numbers. Sādhanā 45: 107 DOI https://doi.org/10.1007/s12046-020-01358-6
22. Chaitanya NVVK, Chatterjee D (2021) Influence of counter rotation on fluid flow and heat transfer around tandem circular

cylinders at low Reynolds number. Journal of the Brazilian Society of Mechanical Sciences and Engineering 43: 357 DOI https://doi.org/10.1007/s40430-021-03072-8

23. Chaitanya NVVK, Chatterjee D, Mondal B (2023) The role of cross thermal buoyancy on flow transition around side-by-side cylinders at low Reynolds numbers. Journal of Thermal Analysis and Calorimetry148:2921-2931DOI https://doi.org/10.1007/s10973-022-11620-0
24. Dey P, Das AK (2015) Numerical analysis of drag and lift reduction of square cylinder. Engineering Science and Technology, an International Journal 18: 758-768DOI https://doi.org/10.1016/j.jestch.2015.05.007
25. Rastan MR, Alam MM, Zhu H, Ji C (2022) Onset of vortex shedding from a bluff body modified from square cylinder to normal flat plate. Ocean Engineering 244:110393DOI https://doi.org/10.1016/j.oceaneng.2021.110393
26. Roadman RE, Loehrke RI (1983) Low Reynolds number flow between interrupted flat plates. Journal of Heat Transfer105:166-171DOI https://doi.org/10.1115/1.3245536
27. Suksangpanomrung A, Chungpaibulpatana S, Promvonge P (2007) Numerical investigation of heat transfer in pulsating flows through a bluff plate. International Communications in Heat and Mass Transfer34:829-837DOI https://doi.org/10.1016/j.icheatmasstransfer.2007.03.013
28. Zhou Y, Zhang L, Bu S, Sun C, Xu W, Xiao Y, Liu L (2020) Study on heat transfer characteristics of the whole plate fin tube cooler. International Journal of Thermofluid Science and Technology 7: 070204DOI https://doi.org/10.1115/1.3245537/10.36963/IJTST.2020070204
29. El Khchine Y, Sriti M (2023) Unsteady forced convection flow and heat transfer past a blunt headed semicircular cylinder at low Reynolds numbers. Numerical Heat Transfer, Part A: Applications 83: 69-79 DOI https://doi.org/10.1080/01457632.2022.2083880
30. Tian X, Ong MC, Yang J, Myrhaug D (2014) Large-eddy simulation of the flow normal to a flat plate including corner effects at a high Reynolds number. Journal of Fluids and Structures 49: 149-169 DOI https://doi.org/10.1016/j.jfluidstructs.2014.04.008
31. Hiramatsu M, Ishimaru T, Ohkouch T (1992) Numerical analysis of innerfins for intercoolers. JSME international journal Ser 2, Fluids engineering, heat transfer, power, combustion, thermophysical properties35:406-412DOI https://doi.org/10.1299/jsmeb1988.35.3_406
32. Ghajar AJ, Yunus A. Cengel D (2015) Heat and Mass Transfer: Fundamentals and Applications McGraw-Hill Education
33. Manglik RM, Bergles AE (1995) Heat transfer and pressure drop correlations for the rectangular offset strip fin compact heat exchanger. Experimental Thermal and Fluid Science 10: 171-180 DOI https://doi.org/10.1016/0894-1777(94)00096-Q